


# Coexistence of giant Rashba splitting, multiple band inversion, and multiple Dirac surface states in the three-dimensional topological insulator $X\text{SnBi}$ ( $X=\text{Rb}, \text{Cs}$ )

Shivendra Kumar Gupta <sup>\*</sup>, Ashish Kore , Saurabh Kumar Sen , and Poorva Singh <sup>†</sup>  
*Department of Physics, Visvesvaraya National Institute of Technology, Nagpur, 440010, India*

 (Received 8 November 2022; revised 1 February 2023; accepted 3 February 2023; published 21 February 2023)

Composite quantum compounds (CQCs) have emerged as a key tool for examining the interactions between two different physical phenomena. Some of these CQCs that have lately received a lot of community attention are topological superconductors and axion insulators, among others. Despite being two distinct quantum phenomena, Rashba spin physics and topological nontriviality can coexist in a CQC platform. In this work, we have performed *ab initio* calculations to discover materials that inherit both giant Rashba splitting and topological nontrivial states in a single crystalline system, coined as intrinsic CQCs. In this regard, we have investigated two materials,  $\text{RbSnBi}$  and  $\text{CsSnBi}$ , that are found to be strong topological insulators along with giant Rashba splitting energy in valence bands (133 and 228 meV, respectively) with Rashba coefficient  $\alpha_R$  to be 4.26 and 6.4 eV Å, respectively. These values of  $\alpha_R$  are quite large, and the Rashba coefficient of  $\text{CsSnBi}$  is the largest, corresponding to valence bands, among previously reported topological materials. Coexisting characteristics of Rashba spin physics and topological nontriviality have the potential to unveil new physical phenomena. For both  $\text{RbSnBi}$  and  $\text{CsSnBi}$ , the topological insulating state is found to be associated with coexisting multiple band inversion and multiple Dirac surface states.

DOI: [10.1103/PhysRevB.107.075143](https://doi.org/10.1103/PhysRevB.107.075143)

## I. INTRODUCTION

A topological insulator (TI) is a material with a nontrivial Dirac surface state crossing the Fermi level and exchange of band characteristics between the valence and the conduction band. This results in the dissipationless spin transport through the edges while the material remains insulating from the bulk [1–4]. The topological insulators are characterized by a nonzero  $Z_2$  topological invariant, signifying the odd number of gapless spin-helical topological surface states (TSS) protected by time-reversal symmetry (TRS) [5–7]. These materials are promising candidates for various applications like spintronics, quantum computing, high-performance infrared detectors, and thermoelectric devices [8].

Though one pair of exchange of band characteristics (single band inversion) and one Dirac surface state is enough for a material to be topological with nonzero  $Z_2$  invariant [9–12], multiple band inversion and multiple Dirac surface states are special features. Multiple band inversion is one of the novel phenomena in topological insulators and has been recently reported in a topological excitonic insulator  $\text{Ta}_2\text{NiSe}_5$  with two different phases, namely, orthorhombic and monoclinic. The multiple  $p-d$  and  $d-d$  type band inversions are present even when spin-orbit coupling (SOC) strength was not included, while the SOC-induced band inversion is only present in the monoclinic phase at the  $\Gamma$  point [13]. Multiple Dirac surface states have been reported theoretically in the topological metal  $\text{LaBi}$  at the (001) surface, two at the

$M$  point and one at the  $\Gamma$  point [14]. A different approach leading to multiple Dirac surface states is via construction of multiple layered structures, giving rise to the surface states corresponding to each layer in the composite system, as reported by Papagno *et al.* [15]. The multiple layered structure of  $\text{PbBi}_6\text{Te}_{10}$  consisted of combination of septuple layers and quintuple layers in a particular sequence such that the three distinct surface terminations resulted in multiple Dirac cones, centered at the  $\Gamma$  point, having similar characteristics to two-dimensional individual layered surface states [15]. Until now, multiple band inversion and multiple Dirac surface states have been observed separately [13–15]; however, these can be intertwined in some materials, as the band inversion is a prerequisite and surface state is a hallmark of TI.

In the search for new quantum phenomena and to gain understanding about the intrinsic nature of the quantum materials, composite quantum compounds (CQCs) are one of the most promising materials. The underlying concept behind CQCs is to combine two or more distinct phenomena in physics together in a single crystal [16,17]. A variety of attempts have been made to discover CQCs with different pairs of phenomena, e.g., combining topology and superconductivity leads to a topological superconductor which is an excellent candidate for generating distinct qubits for quantum computing [18,19]. Merging topological characteristic with magnetism leads to a topological axion insulator which shows quantized magnetoelectric effects and a magnetic topological insulator [20–22]. Topological insulators along with giant Rashba spin splitting, another combination of two distinct quantum phenomena together in a single material [23–25], within the regime of CQCs, leads to the emergence of rich phenomena. For instance, two different topological phases,

<sup>\*</sup>shivendrakumarg900@gmail.com

<sup>†</sup>poorvasingh@phy.vnit.ac.in

Weyl semimetal and TI, coexist in the doped single matrix polar compound  $\text{KSnSb}_x\text{Bi}_{1-x}$  [17] and  $\text{KMgSb}_x\text{Bi}_{1-x}$  [24]. The discovery of intrinsic CQCs, on the other hand, that already possess topological insulating properties and are accompanied by giant Rashba splitting may result in richer physics and potentially undiscovered phenomena.

An important application of CQC materials is in the field of spintronics, where dissipationless spin current is present in topological material with large Rashba splitting. Rashba splitting was first recognized by Rashba, who commented that if asymmetric electric potential breaks inversion symmetry, SOC creates an effective magnetic field, resulting in the breaking of the degeneracy of spin and polarized bands [26–28]. The magnitude of the Rashba coefficient is the ratio of spin splitting energy  $\Delta E$  and the momentum offset  $\Delta K$ , i.e.,  $\alpha_R = 2\Delta E/\Delta K$ . The Rashba splitting is generally considered as “giant” when the energy scale is of the order of or greater than 100 meV [29]. A noncentrosymmetric structure with local electric dipoles induced by polar atomic sites is crucial for the Rashba effect, and band anticrossing is a hallmark of a strong  $\alpha_R$  [28]. Large  $\alpha_R$  implies large energy splitting between spin-up and spin-down states, making it useful in spintronics and current-induced switching in memory and logic devices [30]. It also enhances spin-momentum locking, which can be useful in topological quantum computing and quantum information processing [30]. Additionally, giant  $\alpha_R$  leads to enhanced spin-Hall conductivity [31] and spin-Hall angle [32], and enables easier manipulation of electronic spin without the external magnetic field [33,34], potentially leading to more energy-efficient spintronics technologies and control of electronic transport properties in devices.

In the present study, electronic properties of computationally predicted  $n$ -type thermoelectric material  $X\text{SnBi}$  (where  $X = \text{Rb}, \text{Cs}$ ) [35] have been investigated via first-principles calculations. The study reveals that  $\text{RbSnBi}$  and  $\text{CsSnBi}$  possess giant Rashba splitting and also show properties indicative of a strong topological insulator, similar to  $\text{KSnBi}$ , which has already been reported as a strong topological insulator with a weak Rashba splitting ( $\alpha_R = 1.34$ ). The topological properties of  $\text{RbSnBi}$  and  $\text{CsSnBi}$  have also been confirmed by  $Z_2$  topological number and Dirac surface states. Further investigation leads to multiple band inversion in both  $\text{RbSnBi}$  and  $\text{CsSnBi}$ , which is confirmed by multiple surface states crossing the Fermi level and corresponding Fermi ring. Hence, both materials are predicted to be intrinsic CQCs, where topological insulating behavior coexists with giant Rashba splitting. Interestingly, multiple band inversion and multiple Dirac surface states occur simultaneously in the respective single crystal of  $\text{RbSnBi}$  and  $\text{CsSnBi}$ .

## II. RESULTS AND DISCUSSION

The  $n$ -type thermoelectric material  $\text{RbSnBi}$  ( $\text{CsSnBi}$ ) belongs to space group  $P6_3mc$  (186) and possesses a hexagonal crystal structure with optimized lattice parameter  $a = 4.61 \text{ \AA}$  and  $c = 13.95 \text{ \AA}$  ( $a = 4.69 \text{ \AA}$  and  $c = 14.33 \text{ \AA}$ ) as shown in Fig. 1(a). The absence of imaginary phonon frequencies has demonstrated the dynamic stability of both materials [35]. The potential imbalance present in the structure leads to giant Rashba spin splitting in the  $M - \Gamma$

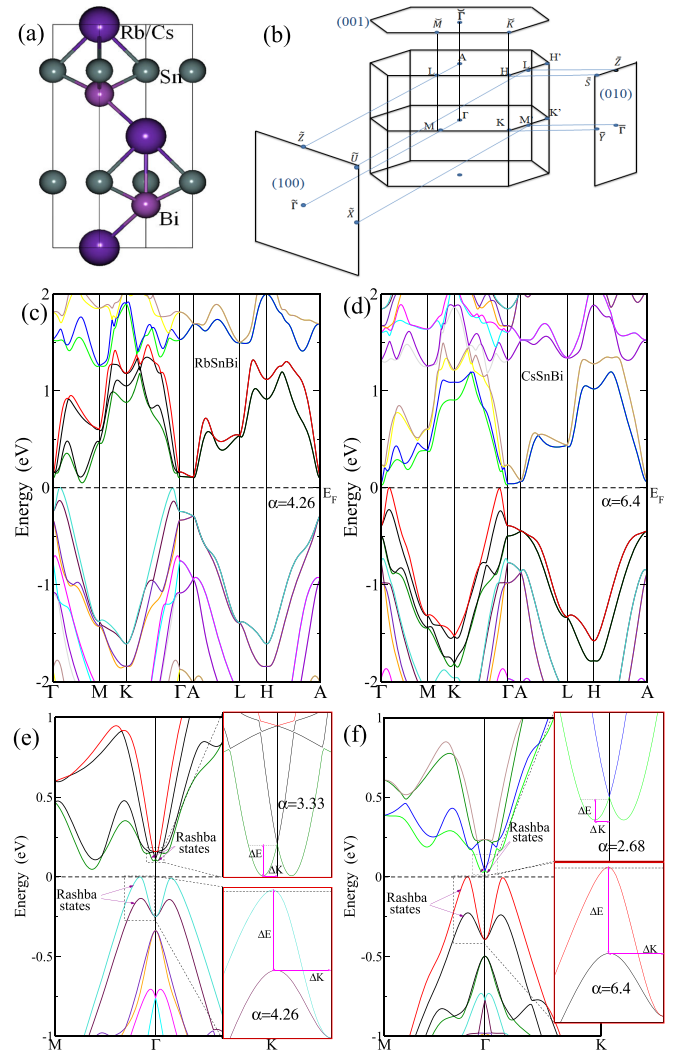


FIG. 1. (a) Crystal structure of  $\text{RbSnBi}$  and  $\text{CsSnBi}$ . (b) Bulk and surface Brillouin zone [(100),(010),(001)] of hexagonal structure. SOC-induced electronic bulk band structure of (c)  $\text{RbSnBi}$  and (d)  $\text{CsSnBi}$ . The SOC-induced electronic band structure for  $M - \Gamma - K$  path representing the Rashba splitting and Rashba coefficient in valance and conduction band for (e)  $\text{RbSnBi}$  and (f)  $\text{CsSnBi}$  and magnified image of Rashba bands is shown for both valance and conduction band.

and  $\Gamma - K$  path in the Brillouin zone. The three-dimensional (3D) and two-dimensional (2D) Brillouin zones are shown in Fig. 1(b). The electronic band structure of  $\text{RbSnBi}$  and  $\text{CsSnBi}$  including SOC strength is shown in Figs. 1(c) and 1(d), which have band anticrossing in the spin-splitting band that gives rise to large Rashba splitting in both the valance band and conduction band. The giant Rashba splitting energy  $\Delta E$  and Rashba coefficient  $\alpha_R$  in the valance band for  $\text{RbSnBi}$  ( $\text{CsSnBi}$ ) are 133 meV and 4.26 eV  $\text{\AA}$  (228 meV and 6.4 eV  $\text{\AA}$ ), where as Rashba splitting energy  $\Delta E$  and Rashba coefficient  $\alpha_R$  in the conduction band for  $\text{RbSnBi}$  ( $\text{CsSnBi}$ ) are 12.5 meV and 3.33 eV  $\text{\AA}$  (12.6 meV and 2.68 eV  $\text{\AA}$ ), respectively, as shown in Figs. 1(e) and 1(f). The magnified image of the Rashba bands is shown for the identification of  $\Delta E$  and  $\Delta K$ . The values of  $\alpha$  in

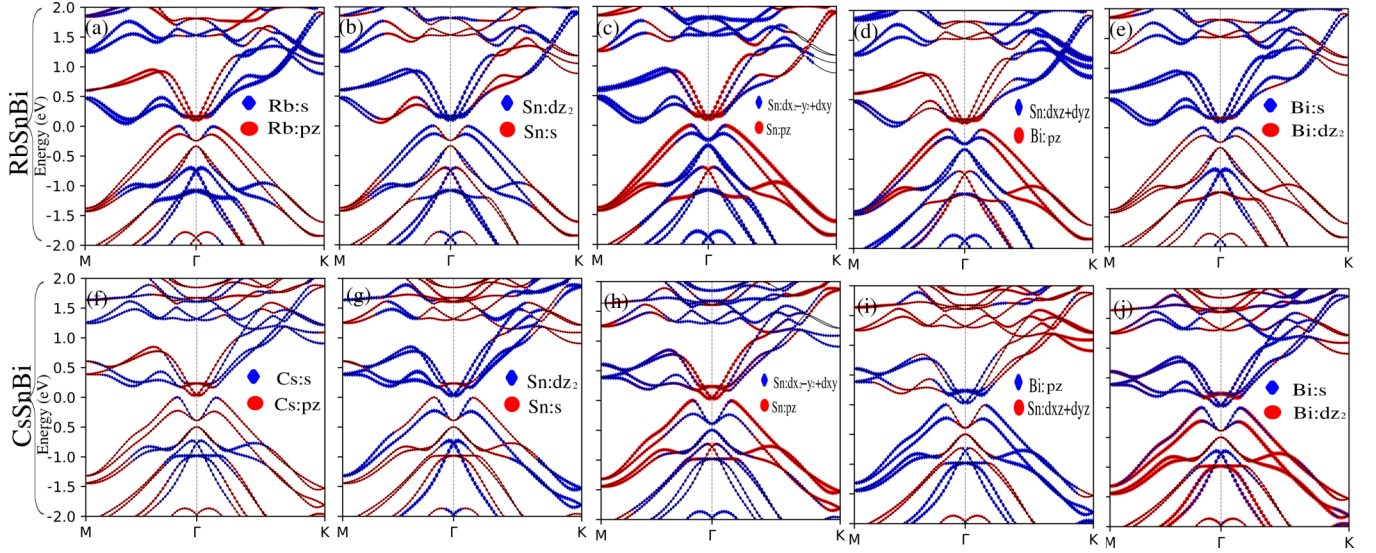


FIG. 2. Multiple band inversion in RbSnBi including SOC strength: (a) Rb: $s$  and Rb: $p_z$ , (b) Sn: $s$  and Sn: $d_{z^2}$ , (c) Sn: $p_z$  and Sn: $d_{x^2-y^2} + d_{xy}$ , (d) Sn: $d_{xz} + d_{yz}$  and Bi: $p_z$ , and (e) Bi: $s$  and Bi: $d_{z^2}$ . Multiple band inversion in CsSnBi including SOC strength: (f) Cs: $s$  and Cs: $p_z$ , (g) Sn: $s$  and Sn: $d_{z^2}$ , (h) Sn: $p_z$  and Sn: $d_{x^2-y^2} + d_{xy}$ , (i) Sn: $d_{xz} + d_{yz}$  and Bi: $p_z$ , and (j) Bi: $s$  and Bi: $d_{z^2}$ .

the valence band are quite large; especially, the  $\alpha$  value of CsSnBi is much larger than KSnSb $_x$ Bi $_{1-x}$  ( $\alpha_R = 4.83$  eV $\text{\AA}$ ) [17], BiTeI ( $\alpha_R = 4.548$  eV $\text{\AA}$ ), GeTe ( $\alpha_R = 4.352$  eV $\text{\AA}$ ), BiTeCl ( $\alpha_R = 3.564$  eV $\text{\AA}$ ), Sb $_2$ TeSe $_2$  ( $\alpha_R = 3.885$  eV $\text{\AA}$ ) [28], which suggests that RbSnBi and CsSnBi are ideal candidates for intrinsic CQCs.

Projected band structures for RbSnBi and CsSnBi are presented in Figs. 2(a)–2(j) showing multiple band inversion. We observe five different pairs of band exchange characteristics, with multiple bands in each pair as shown by orbital weightage. The  $s - p$ ,  $s - d$ , and  $p - d$  multiple band inversions are present in both RbSnBi and CsSnBi even when SOC is not included in the system. When SOC strength is included, the degeneracy of the bands breaks, and the band inversion is present in spin-split bands. The weightage of  $s$  and  $p_z$  orbitals of Rb atoms depicts the interchange of their band characteristics as shown in Fig. 2(a). Similar multiple band character exchange phenomena are seen in  $s$  and  $d_{z^2}$  orbitals of Sn atoms [Fig. 2(b)]. The bands are also inverted between the  $p_z$  orbital and  $d_{x^2-y^2} + d_{xy}$  orbital of Sn atoms [Fig. 2(c)]. Additionally, the band inversion can be observed between the  $d_{xz} + d_{yz}$  orbital of Sn atoms with  $p_z$  orbitals of Bi atoms [Fig. 2(d)]. Band inversion is also present in the  $s$  and  $d_{z^2}$  orbitals of Bi atoms, shown in Fig. 2(e). Similarly, for CsSnBi multiple band inversion includes the  $s$  and  $p_z$  orbitals of Cs atoms in Fig. 2(f), the  $s$  and  $d_{z^2}$  orbitals of Sn atoms in Fig. 2(g), the  $p_z$  and  $d_{x^2-y^2} + d_{xy}$  orbitals of Sn atoms in Fig. 2(h), the  $p_z$  orbital of Bi and  $d_{xz+yz}$  orbital of Sn atoms in Fig. 2(i), and the  $s$  and  $d_{z^2}$  orbitals of Bi atoms in Fig. 2(j).

As band inversion is a prerequisite for TI, we first determine the  $Z_2$  invariant number using the Wannier charge center (WCC) to corroborate the topological insulating nature of the material. The representation of Wilson flow of WCC for the six-time reversal invariant momentum plane for  $k_i = 0$  and  $0.5$  [ $i = 1, 2, 3$ ] for RbSnBi is shown in Figs. 3(a)–3(f) and for CsSnBi is shown in Figs. 3(g)–3(l). In Figs. 3(a), 3(c) and 3(e), where  $k_i = 0$ , the odd number of WCC evaluation lines

(green lines) crossing the horizontal reference line (red dashed line) results in  $Z_2 = 1$ , whereas in Figs. 3(b), 3(d) and 3(f), where  $k_i = 0.5$ , the even number of WCC evaluation lines crossing the horizontal reference line gives  $Z_2 = 0$ . Similarly, for CsSnBi in Figs. 3(g), 3(i), and 3(k), where  $k_i = 0$ , the odd number of evaluation lines crossing the horizontal reference line gives  $Z_2 = 1$ , whereas in Figs. 3(h), 3(j), and 3(l), where  $k_i = 0.5$ , the even number of WCC evaluation lines crossing the horizontal reference line results in  $Z_2 = 0$ .

The  $Z_2$  invariant is indicated as  $(\nu_0; \nu_1 \nu_2 \nu_3)$ , where  $\nu_0, \nu_1, \nu_2, \nu_3$  are four distinct  $Z_2$  invariants where  $\nu_0 = [Z_2(k_i = 0) + Z_2(k_i = 0.5)] \bmod 2$  and  $\nu_i = Z_2(k_i = 0.5)$ . According to these values, topological materials are categorized into strong TI, weak TI, and trivial insulators. If  $\nu_0 = 1$ , then the material is a strong TI, whereas if  $\nu_0 = 0$ , and at least one among the  $\nu_1, \nu_2$ , and  $\nu_3$  is nonzero, then the material is a weak TI; however, if all  $\nu_0, \nu_1, \nu_2$ , and  $\nu_3$  are zero, this indicates a trivial insulator. The  $Z_2$  invariant calculated in this way is (1000) for both RbSnBi and CsSnBi, indicating that both materials are strong topological insulators.

Further, we calculate the surface band structure of RbSnBi and CsSnBi, suspecting that the multiple band inversion may lead to multiple surface Dirac states in these materials. In this regard, we calculate the surface band structure of (001), (010), and (100) surfaces. For RbSnBi, we calculate the (001) surface band structure (Rb-terminated) and observe the surface state crossing the Fermi level at the  $\Gamma$  point [Fig. 4(a)], and its corresponding Fermi ring is shown in Fig. 4(b). There is a ring at the  $\Gamma$  point to indicate the topological surface state, and an additional ring corresponds to the surface state crossing the bulk region of the conduction band between the M and  $\Gamma$  point [represented by the black dashed circle in Fig. 4(a)]. Figures 4(c) and 4(d) show the (100) surface band structures of RbSnBi at  $Z - \Gamma - Z$  and  $X - \Gamma - X$  paths, respectively, having the surface state crossing the Fermi level at the  $\Gamma$  point. The surface state also crosses the conduction bulk region at both sides of the  $\Gamma$  point represented by the black dashed



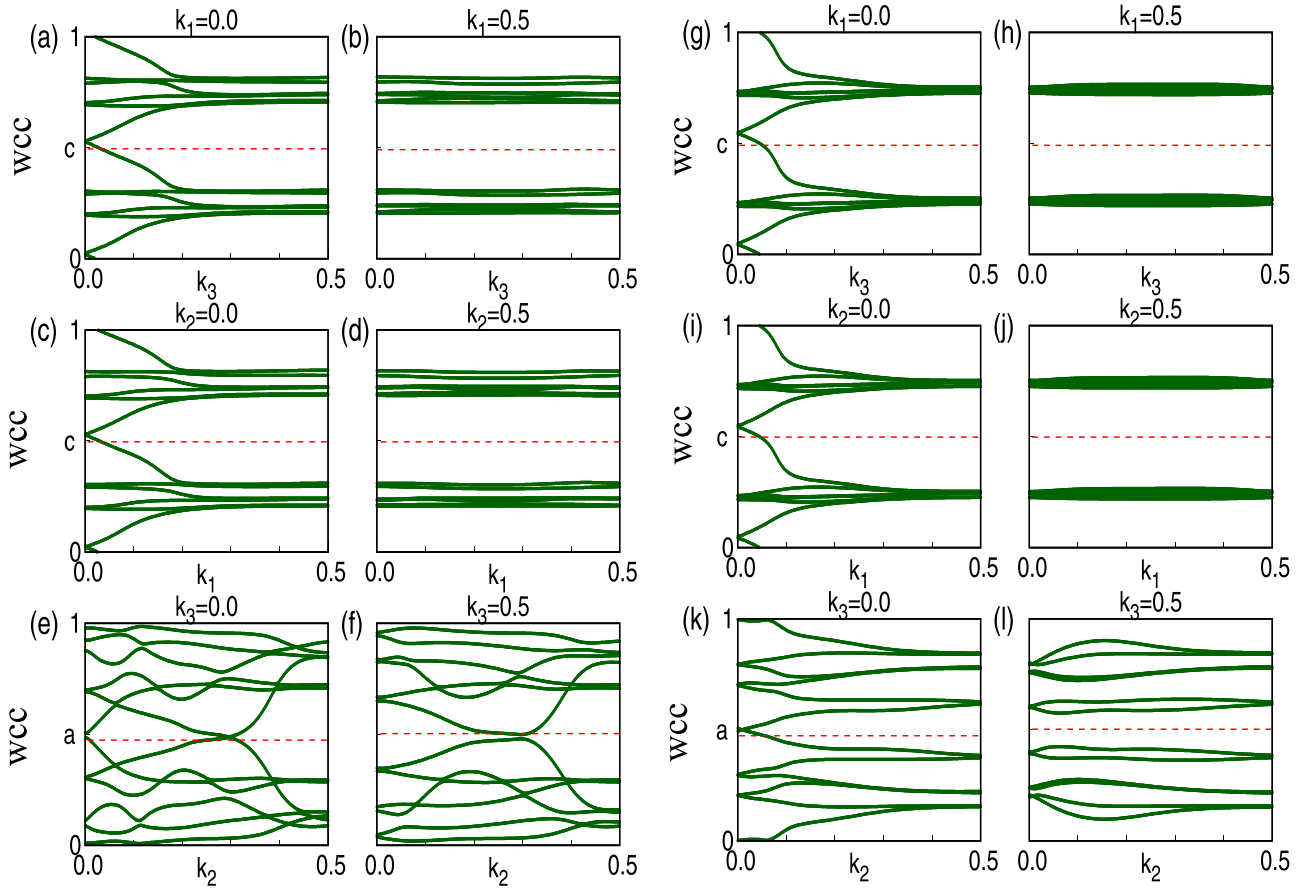


FIG. 3. The Wilson loop for RbSnBi in the time-reversal invariant plane (TRIP) along (a)  $k_1 = 0.0$ , (b)  $k_1 = 0.5$ , (c)  $k_2 = 0.0$ , (d)  $k_2 = 0.5$ , (e)  $k_3 = 0.0$ , and (f)  $k_3 = 0.5$ . The Wilson loop for CsSnBi in TRIP along (g)  $k_1 = 0.0$ , (h)  $k_1 = 0.5$ , (i)  $k_2 = 0.0$ , (j)  $k_2 = 0.5$ , (k)  $k_3 = 0.0$ , and (l)  $k_3 = 0.5$ .

circles in Fig. 4(d). The surface ring corresponding to the (100) surface for RbSnBi is shown in Fig. 4(e). There are three Fermi rings merged together and taking the form of an asymmetric dumbbell, one representing the crossing at the  $\Gamma$  point and two representing the surface state crossing the conduction bulk band at both sides of the  $\Gamma$  point. Figure 4(g) shows the (010) surface band structure of the Sn<sub>2</sub>-terminated surface of CsSnBi, which has a surface state crossing the Fermi level at the  $\Gamma$  point, whereas in Fig. 4(f) the (010) surface at path  $Y - \Gamma - Y$  has surface states crossing at three points, one at the  $\Gamma$  point and two crossing at both sides of  $\Gamma$  point. The Fermi ring corresponding to the (010) surface for CsSnBi is shown in Fig. 4(h), where we observe three separate Fermi rings corresponding to three crossing at the  $Y - \Gamma - Y$  surface. These multiple surface states and their corresponding Fermi rings confirm the presence of the multiple band inversion in both materials.

### III. COMPUTATIONAL METHODS

Electronic properties of  $X$ SnBi compounds have been investigated by the first-principles calculation based on standard density functional theory with the full potential linearized augmented plane-wave method provided by the WIEN2K package [36]. Generalized gradient approximation (GGA) with projector augmented wave (PAW) potentials have been

utilized to incorporate the exchange-correlation function.  $R_{\text{MTK}_{\text{max}}}$  was set to 6.5 to acquire the plane wave cutoff. The  $12 \times 12 \times 4$  k-mesh is used to perform self-consistent calculations (SCF). Maximally localized Wannier functions (MLWF) are used to develop the tight binding model, which is used to calculate the surface states of the materials using WANNIER90 code [37]. WANNIERTOOLS is used to obtain topological characteristics such as Wilson loops (Wannier charge centers),  $Z_2$  invariants, topological surface state, and Fermi surface ring [38].

### IV. CONCLUSION

In conclusion, we employ the first-principles calculations to search for intrinsic CQC materials that possess both the topological nontrivial characteristic and giant Rashba splitting, accompanied by multiple band inversion and multiple Dirac surface states. Large spin-orbital coupling due to heavy elements, breaking of inversion symmetry, and the band anticrossing imposed on the system leads to giant Rashba splitting. We predict two intrinsic CQCs:  $n$ -type thermoelectric materials RbSnBi and CsSnBi, possessing topological nontrivial states, and giant Rashba splitting. Additionally, the Rashba coefficient of RbSnBi in the valence band is quite large ( $\alpha_R = 4.26$  and  $6.4$  eV  $\text{\AA}$ , respectively). CsSnBi has the largest Rashba coefficient in the valence band reported so

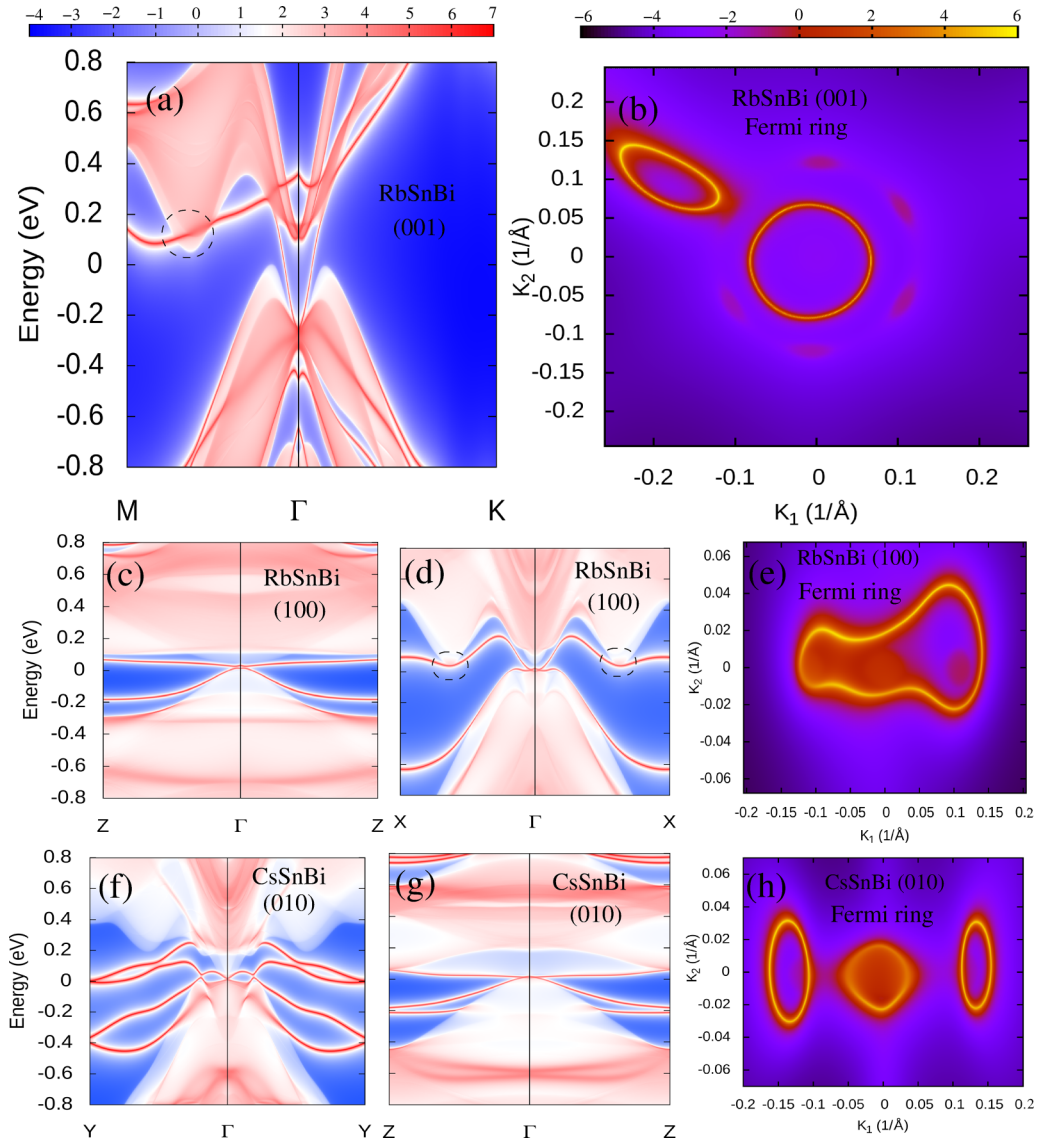


FIG. 4. Surface state of RbSnBi: (a) (001) plane at  $M - \Gamma - K$  and (b) Fermi ring corresponding to (001) surface. The surface state of RbSnBi (100) surface: (c)  $Z - \Gamma - Z$ , (d)  $X - \Gamma - X$ , and (e) Fermi ring corresponding to (100) surface. Surface state of CsSnBi (010) surface: (f)  $Y - \Gamma - Y$ , (g)  $Z - \Gamma - Z$ , and (h) Fermi ring corresponding to (010) surface.

far, making it an ideal candidate for further investigation by experimental means. Wannier charge center based investigation yields  $Z_2$  invariant (1000) for both the materials, indicating that the materials are strong topological insulators. These  $n$ -type thermoelectric materials having a strong topological nature with multiple surface Dirac states may have unique properties that could be used in various applications. Multiple Dirac surface states can host several exotic physical phenomena, such as chiral anomaly and negative

magnetoresistance, which can be exploited for a variety of applications in spintronics and quantum computing. We anticipate that the findings presented here will encourage physicists to investigate these materials experimentally.

#### ACKNOWLEDGMENT

Author P.S. would like to thank NPSF C-DAC Pune for providing the HPC facility.

[1] C.-Z. Chang, P. Z. Tang, X. Feng, K. Li, X.-C. Ma, W. H. Duan, K. He, and Q.-K. Xue, Band Engineering of Dirac Surface States in Topological-Insulator-Based van der Waals Heterostructures, *Phys. Rev. Lett.* **115**, 136801 (2015).

[2] S. Mukherjee, S. W. Jung, S. F. Weber, C. Xu, D. Qian, X. Xu, P. K. Biswas, T. K. Kim, L. C. Chapon, M. D. Watson, J. B. Neaton, and C. Cacho, Fermi-crossing Type-II Dirac fermions and topological surface states in  $\text{NiTe}_2$ , *Sci. Rep.* **10**, 12957 (2020).

- [3] Y. D. Ma, L. Z. Kou, Y. Dai, and T. Heine, Proposed two-dimensional topological insulator in SiTe, *Phys. Rev. B* **94**, 201104(R) (2016).
- [4] M. Khazaei, A. Ranjbar, M. Arai, and S. Yunoki, Topological insulators in the ordered double transition metals  $M_2MC_2$  MXenes ( $M = Mo, W$ ;  $M = Ti, Zr, Hf$ ), *Phys. Rev. B* **94**, 125152 (2016).
- [5] A. P. Weber, Q. D. Gibson, Huiwen Ji, A. N. Caruso, A. V. Fedorov, R. J. Cava, and T. Valla, Gapped Surface States in a Strong-Topological-Insulator Material, *Phys. Rev. Lett.* **114**, 256401 (2015).
- [6] Y. Xu, I. Miotkowski, C. Liu, J. Tian, H. Nam, N. Alidoust, J. Hu, C.-K. Shih, M. Z. Hasan, and Y. P. Chen, Observation of topological surface state quantum Hall effect in an intrinsic three-dimensional topological insulator, *Nat. Phys.* **10**, 956 (2014).
- [7] S. V. Eremeev, T. V. Menshchikova, I. V. Silkin, M. G. Vergniory, P. M. Echenique, and E. V. Chulkov, Sublattice effect on topological surface states in complex  $(SnTe)_n > 1 (Bi_2Te_3)_m = 1$  compounds, *Phys. Rev. B* **91**, 245145 (2015).
- [8] W. Tian, W. Yu, J. Shi, and Y. Wang, The property, preparation and application of topological insulators: A review, *Materials* **10**, 814 (2017).
- [9] A. Kore, N. Ara, and P. Singh, First principle based investigation of topological insulating phase in half-Heusler family NaYO ( $Y = Ag, Au, \text{ and } Cu$ ), *J. Phys.: Condens. Matter* **34**, 205501 (2022).
- [10] M. M. H. Polash, S. Yalameha, H. Zhou, K. Ahadi, Z. Nourbakhsh, and D. Vashaee, Topological quantum matter to topological phase conversion: Fundamentals, materials, physical systems for phase conversions, and device applications, *Mater. Sci. Eng. R Rep.* **145**, 100620 (2021).
- [11] S.-Y. Lin, M. Chen, X.-B. Yang, Y.-J. Zhao, S.-C. Wu, C. Felser, and B. Yan, Theoretical search for half-Heusler topological insulators, *Phys. Rev. B* **91**, 094107 (2015).
- [12] S. M. Singh, R. Kumar, S. Srivastava, T. Kumar, Structural, electronic and topological properties of NaCaBi and KBaBi compounds, *J. Phys. Chem. Solids* **161**, 110416 (2022).
- [13] X. Ma, G. Wang, H. Mao, Z. Yuan, T. Yu, R. Liu, Y. Peng, P. Zheng, and Z. Yin,  $Ta_2NiSe_5$ : A candidate topological excitonic insulator with multiple band inversions, *Phys. Rev. B* **105**, 035138 (2022).
- [14] J. Nayak, S.-C. Wu, N. Kumar, C. Shekhar, S. Singh, J. Fink, E. E. D. Rienks, G. H. Fecher, S. S. P. Parkin, B. Yan, and C. Felser, Multiple Dirac cones at the surface of the topological metal LaBi, *Nat. Commun.* **8**, 13942 (2017).
- [15] M. Papagno, S. V. Eremeev, J. Fujii, Z. S. Aliev, M. B. Babanly, S. K. Mahatha, I. Vobornik, N. T. Mamedov, D. Pacilé, and E. V. Chulkov, Multiple coexisting Dirac surface states in three-dimensional topological insulator  $PbBi_6Te_7$ , *ACS Nano* **10**, 3518 (2016).
- [16] C.-H. Hsu, P. C. Sreeparvathy, C. K. Barman, F.-C. Chuang, and A. Alam, Coexistence of topological nontrivial and spin-gapless semiconducting behavior in  $MnPO_4$ : A composite quantum compound, *Phys. Rev. B* **103**, 195143 (2021).
- [17] C. Mondal, C. K. Barman, A. Alam, and B. Pathak, Intertwined nontrivial band topology and giant Rashba spin splitting, *Phys. Rev. B* **104**, 085113 (2021).
- [18] M. Z. Hasan and C. L. Kane, Colloquium: Topological insulators, *Rev. Mod. Phys.* **82**, 3045 (2010).
- [19] X.-L. Qi and S.-C. Zhang, Topological insulators and superconductors, *Rev. Mod. Phys.* **83**, 1057 (2011).
- [20] Y. S. Hou, J. W. Kim, and R. Q. Wu, Axion insulator state in ferromagnetically ordered  $CrI_3/Bi_2Se_3/MnBi_2Se_4$  heterostructures, *Phys. Rev. B* **101**, 121401(R) (2020).
- [21] J.-H. Li, Y. Li, S. Du, Z. Wang, B.-L. Gu, S.-C. Zhang, K. He, W. Duan, and Y. Xu, Intrinsic magnetic topological insulators in van der Waals layered  $MnBi_2Te_4$ -family materials, *Sci. Adv.* **5**, eaaw5685 (2019).
- [22] C. Liu, Y. Wang, H. Li, Y. Wu, Y. Li, J. Li, K. He, Y. Xu, J. Zhang, and Y. Wang, Robust axion insulator and Chern insulator phases in a two-dimensional antiferromagnetic topological insulator, *Nat. Mater.* **19**, 522 (2020).
- [23] K. Ishizaka, M. Bahramy, H. Murakawa, M. Sakano, T. Shimojima, T. Sonobe, K. Koizumi, S. Shin, H. Miyahara, A. Kimura *et al.*, Giant Rashba-type spin splitting in bulk BiTeI, *Nat. Mater.* **10**, 521 (2011).
- [24] D. Di Sante, P. Barone, A. Stroppa, K. F. Garrity, D. Vanderbilt, and S. Picozzi, Intertwined Rashba, Dirac, and Weyl Fermions in Hexagonal Hyperferroelectrics, *Phys. Rev. Lett.* **117**, 076401 (2016).
- [25] Y. Feng, Q. Jiang, B. Feng, M. Yang, T. Xu, W. Liu, X. Yang, M. Arita, E. F. Schwier, K. Shimada, H. O. Jeschke, R. Thomale, Y. Shi, X. Wu, S. Xiao, S. Qiao, and S. He, Rashba-like spin splitting along three momentum directions in trigonal layered  $PtBi_2$ , *Nat. Commun.* **10**, 4765 (2019).
- [26] E. I. Rashba, Svoistva poluprovodnikov s petlei ekstremumov. I. Tsiklotronnyi i kombinirovannyi rezonans v magnitnom pole, perpendikulyarnom ploskosti petli, *Sov. Phys. Solid State* **2**, 1109 (1960).
- [27] E. I. Rashba and V. I. Sheka, Simmetriya energeticheskikh zon v kristallakh tipa vyurtsita. II. Simmetriya zon s uchyotom spinovykh vzaimodeistvii, *Fiz. Tverd. Tela* **1**, 162 (1959).
- [28] C. M. Acosta, E. Ogoshi, A. Fazzio, G. M. Dalpian, and A. Zunger, The Rashba scale: Emergence of band anti-crossing as a design principle for materials with large Rashba coefficient, *Matter* **3**, 145 (2020).
- [29] M. S. Bahramy, R. Arita, and N. Nagaosa, Origin of giant bulk Rashba splitting: Application to BiTeI, *Phys. Rev. B* **84**, 041202(R) (2011).
- [30] L. Q. Liu, O. J. Lee, T. J. Gudmundsen, D. C. Ralph, and R. A. Buhrman, Current-Induced Switching of Perpendicularly Magnetized Magnetic Layers Using Spin Torque from the Spin Hall Effect, *Phys. Rev. Lett.* **109**, 096602 (2012).
- [31] H. Wang, P. Gopal, S. Picozzi, S. Curtarolo, M. B. Nardelli, and J. Ślawińska, Spin Hall effect in prototype Rashba ferroelectrics GeTe and SnTe, *npj Comput. Mater.* **6**, 7 (2020).
- [32] C. Xiao, Semiclassical Boltzmann theory of spin Hall effects in giant Rashba systems, *Front. Phys.* **13**, 137202 (2018).
- [33] K. Wu, J. Chen, H. Ma, L. Wan, W. Hu, and J. Yang, Two-dimensional giant tunable Rashba semiconductors with two-atom-thick buckled honeycomb structure, *Nano Lett.* **21**, 740 (2021).
- [34] X. Qiu, Z. Shi, W. Fan, S. Zhou, and H. Yang, Characterization and manipulation of spin orbit torque in magnetic heterostructures, *Adv. Mater.* **30**, 1705699 (2018).
- [35] P. Gorai, A. Ganose, A. Faghaninia, A. Jain, and V. Stevanovic, Computational discovery of promising new n-type dopable

- ABX Zintl thermoelectric materials, [Mater. Horiz.](#) **7**, 1809 (2020).
- [36] P. Blaha, K. Schwarz, G. K. H. Madsen, D. Kvasnicka, J. Luitz, R. Laskowski, F. Tran, and L. D. Marks, *WIEN2k: An Augmented Plane Wave Plus Local Orbitals Program for Calculating Crystal Properties* (Vienna University of Technology, Vienna, 2001).
- [37] A. A. Mostofi, J. R. Yates, Y.-S. Lee, I. Souza, D. Vanderbilt, and N. Marzari, wannier90: A tool for obtaining maximally-localised Wannier functions, [Comput. Phys. Commun.](#) **178**, 685 (2008).
- [38] Q. Wu, S. Zhang, H.-F. Song, M. Troyer, and A. A. Soluyanov, Wannertools: An open-source software package for novel topological materials, [Comput. Phys. Commun.](#) **224**, 405 (2018).